Nuclear Inst. and Methods in Physics Research B 461 (2019) 37–43

Contents lists available at ScienceDirect

Nuclear Inst. and Methods in Physics Research B

journal homepage: www.elsevier.com/locate/nimb

Effect of the annealing atmosphere on the layer interdiffusion in Pd/Ti/Pd multilayer stacks deposited on pure Ti and Ti-alloy substrates

Steven Magogodi[a,b], Christopher Mtshali[a,*], Sylvain Halindintwali[b], Zakhelumuzi Khumalo[a], Nametso Mongwaketsi[a], Karen Cloete[a], Moshawe Madito[a], Caswell Pieters[a], Avesh Sook[a], Earl Mc Donald[b], Franscious Cummings[b], Christopher Arendse[b]

[a] iThemba LABS, National Research Foundation, PO Box 722, Somerset West 7129, South Africa
[b] University of the Western Cape, Private Bag X17, Bellville 7535, South Africa

ARTICLE INFO

Keywords:
Palladium-Titanium
Multilayer
Electron beam evaporation
Rutherford backscattering spectrometry
X-ray diffraction
Scanning electron microscope

ABSTRACT

Pd(50 nm)/Ti(25 nm)/Pd(50 nm) multilayer stack has been deposited on Ti and Ti6Al4V substrates; we have studied the intermixing of layers upon annealing at the hydrogenation temperature of 550 °C, under vacuum, H/Ar gas mixture and pure hydrogen atmospheres. Scanning electron microscopy (SEM) micrographs indicated surface roughening in samples annealed under vacuum and H/Ar gas mixture while those annealed under pure H_2 remained relatively smoother. Rutherford backscattering spectrometry (RBS) revealed intermixing of layers as evidenced by the diffusion of Pd toward the bulk, while XRD indicated the formation of $PdTi_2$ phase in the samples annealed under vacuum and H/Ar gas mixture atmosphere. In-situ, real-time RBS showed that the annealing under pure H_2 preserves the integrity of the Pd catalyst. No indication of the $PdTi_2$ formation in the pure H_2 annealed samples was observed; instead only the TiH_2 phase appeared, indicating the absorption of H into the system.

1. Introduction

Ti and Ti6Al4V alloy have attracted much interest from research groups for hydrogen storage applications, due to their high H affinity [1–6]. Titanium and its alloys have found applications in many areas such as in aerospace, marine, etc. due to their corrosion resistance and high strength to weight ratio properties [3]. When used for H storage, Ti and Ti6Al4V alloy have been reported to absorb up to 60 at.% H at 550 °C [6–9]. Many groups have found that the H absorption in Ti and Ti6Al4V systems reaches its optimum at around 550 °C [2,10–15]. Furthermore Fujimoto at al [15] studied the phases formed during hydrogenation of Ti-Pd multilayer at 623 K under vacuum and they reported atomic interlayer mixing and solid state amorphization; however under pure hydrogen gas, they found that only TiH_2 phase was formed. This was supported by Topic at al [12] who concluded also on the TiH_2 formation upon annealing Ti-Pd layer stack deposited onto Ti substrate, at 550 °C.

Hyo-Ryoung Lim et al [16] have also noted interlayer thermal-diffusion during a thermal treatment of < Ti/Ti-Pd (co-sputtered film)/Si (1 0 0) > system; they observed changes in the surface morphology as well as in the compositional distribution of the Pd to Ti ratio of the co-sputtered film, at annealing temperature of 400 °C under vacuum.

Finally, Monika Radlik et al. [17] studied the generation of palladium silicide in the PdAu-SiO_2 nanocomposites during heating in 10% H_2/Ar; from their XRD studies, it was found that high temperatures (> 550 °C) were required to initiate phase transformations of PdAu-SiO_2 while for other systems like PdCu-SiO_2 and Pd-SiO_2, lower temperatures (< 450 °C) were enough. They noted that while the effect of the temperature increase was evident in initiating the phase transformations, prolonged isothermal annealing did yield any new phase.

In this study, we have adopted to anneal a triple layer stack Pd (50 nm)/Ti(25 nm)/Pd(50 nm) deposited on Ti and Ti alloy substrates at the same hydrogenation temperature of 550 °C under three ambient conditions: vacuum, mixed H/Ar and pure H_2 gases. The aim is to probe into the integrity of the layers upon annealing.

2. Materials and experimental methods

Ti and Pd films were deposited onto Ti and Ti6Al4V substrates using a 3 kW high vacuum e-beam evaporation system at room temperature. Substrates were ultrasonically cleaned using acetone and methanol sequentially for duration of 10 min each step. Substrates were then

* Corresponding author.
E-mail address: mtshali@tlabs.ac.za (C. Mtshali).

https://doi.org/10.1016/j.nimb.2019.09.018
Received 30 April 2019; Received in revised form 12 September 2019; Accepted 12 September 2019
Available online 19 September 2019
0168-583X/ © 2019 Elsevier B.V. All rights reserved.

Table 1
Experimental parameters during annealing at 550 °C.

Annealing conditions	Flow rate (sccm)	Time (hours)	Pressure (mbar)
Vacuum	–	2	10^{-6}
H(15%)/Ar(85%)	100	2	10^{-3}
Pure H_2	100	1	10^{-1}

mounted on a non-rotating substrate holder and transferred into the deposition chamber. Pure (99.999%) Ti and Pd pellet targets were placed in separate crucibles for the deposition of Ti and Pd thin films, respectively. The sequential deposition of layers Pd(50 nm)/Ti(25 nm)/Pd(50 nm) was done at a constant deposition rate of 0.6 Å/s and the chamber pressure was kept at 10^{-6} mbar. During deposition, the thickness was monitored using a thickness crystal monitor.

The samples were annealed under three annealing atmospheres at 550 °C: under vacuum at a residual pressure of 10^{-6} mbar; under H(15%)/Ar(85%) gas mixture at 10^{-3} mbar and finally under pure H_2 gas also at 0.1 mbar. The detailed annealing parameters are given in Table 1.

The depth profile and concentration of hydrogen of the as-deposited and hydrogenated samples were measured by ERDA using 3 MeV He^{++} ions emanating from 3 MV Tandetron accelerator based at iThemba Laboratories for accelerator based sciences (iThemba LABS-South Africa). The energy resolution of ERDA depends on the detector resolution but it is affected by the energy straggling in the He^{++} stopping foil, resulting to a value of about 25 keV with a concentration detection limit of 0.1 at.% [18]. The samples were individually mounted on a ladder and then loaded into the sample chamber evacuated to a vacuum pressure better than 10^{-6} mbar. For channel number/energy calibration, the 15 μm thick Kapton standard coated with 1 nm platinum layer in order to avoid charging effects was used. Three spectra were collected using He^{++} beam energies of 2, 2.5 and 3 MeV. Thereafter, the samples were measured using a beam energy of 3 MeV; an average current of ~60 nA and a total collected charge of 40 μC were maintained for all the samples. The energy spectra of recoiled hydrogen

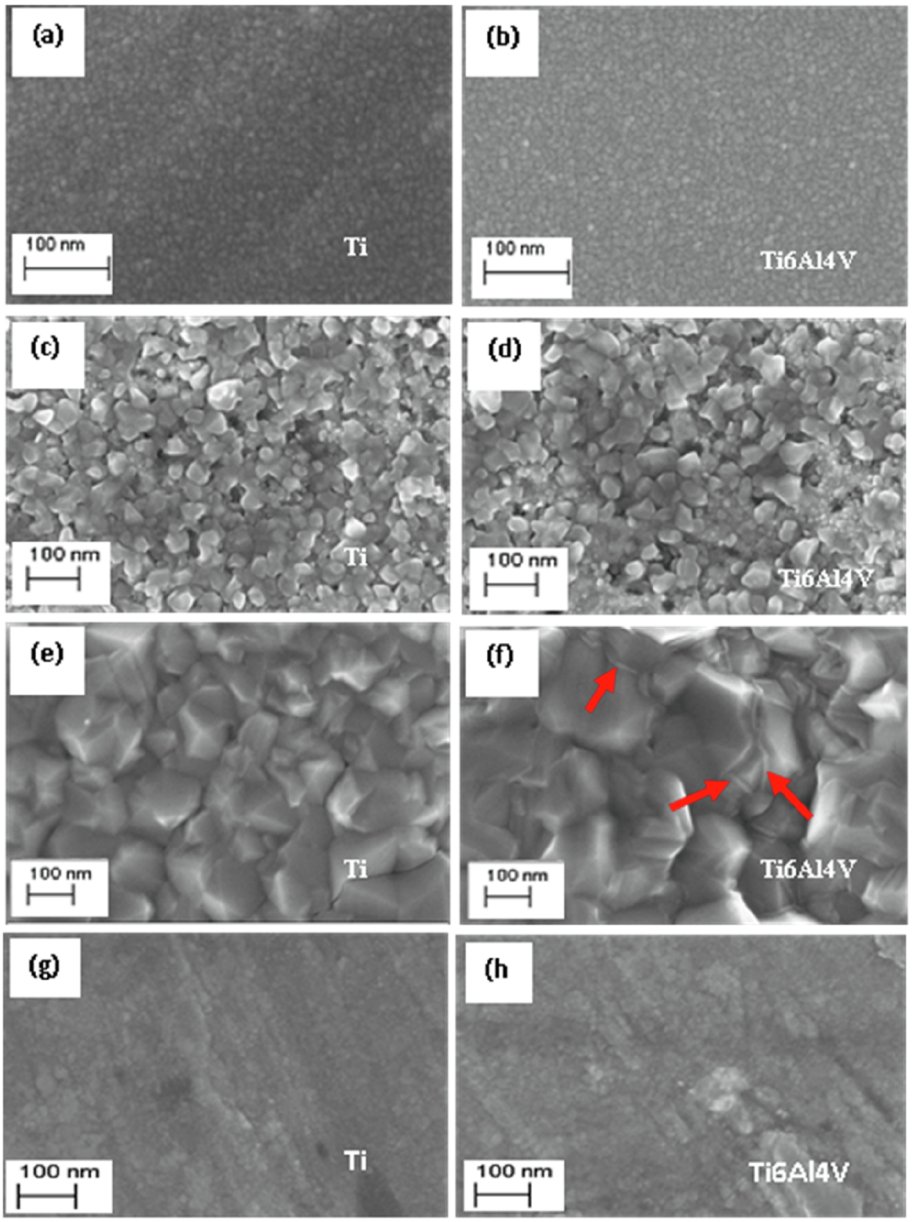

Fig. 1. SEM images of (a-b) as-deposited samples; samples annealed at 550 °C under (c-d) vacuum, (e-f) H(15%)/Ar(85%) gas mixture, and (g-h) pure H_2 (100%) on Ti and Ti6Al4V substrates.

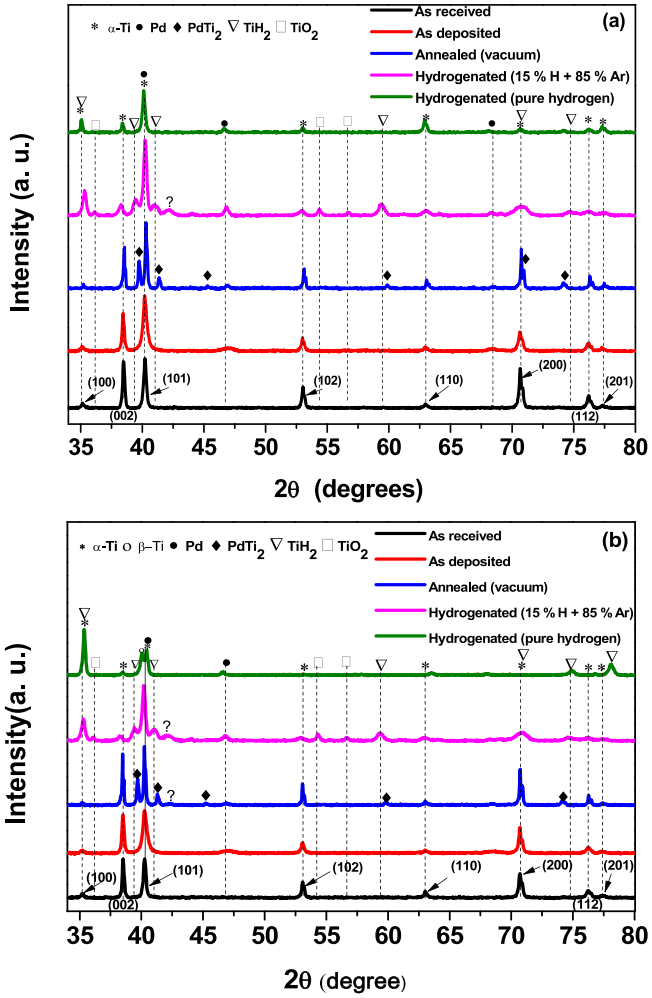

Fig. 2. XRD spectra of the as-deposited samples, samples annealed at 550 °C under vacuum, H(15%)/Ar(85%) gas mixture, and pure H_2 (100%) on (a) Ti and (b) Ti6Al4V substrates.

Table 2
Crystallographic information of different observed phases.

Phase	Pattern no.	Space group	Lattice parameters
α-Ti	00-044-1294	*P63/mmc (1 9 4)*	a = 2.95 nm; c = 4.68 nm
hexagonal β-Ti	00-005-10682	*P63/mmc (1 9 4)*	a = 2.95 nm; c = 4.68 nm
FCC Pd	00-046-1043	*Fm3m (2 2 5)*	a = 3.89 nm
BCC $PdTi_2$	00-010-0057	*I4mmm (1 3 9)*	a = 3.09 nm; c = 10.054 nm
FCC TiH_2	00-025-0982	*Fm3m (2 2 5)*	a = 4.45 nm

atoms were recorded using a Si surface barrier detector with an energy resolution of ~25 keV positioned at a recoiled angle of 30°. The simulation and analysis of ERDA spectra were done using SIMNRA software version 6.06 *[www.simnra.com]*. The non-Rutherford cross section of Baglin (HHeHHe30.R33) [19] in the energy range between 1 and 3 MeV and for a recoiled angle of 30°, was chosen in the simulation process.

2 MeV He^{++} ions were used to collect RBS spectra in all the samples. The channel number calibration in terms of backscattered energy of particles was achieved using a gold-cobalt on top of silicon dioxide deposited on silicon substrate ($AuCo/SiO_2/Si$) standard sample. An average current of 60 nA and total charge of 20 μC were used for all samples. The vacuum pressure during the measurements was better than 10^{-6} mbar. The energy of the scattered He^{++} ions were recorded using a Si surface barrier detector with energy resolution of ~23 keV positioned at a backscattering angle of 150° and the sample surface tilted by 5° towards the detector. Simulations of RBS spectra were achieved using SIMNRA software version 6.06 *[www.simnra.com]* and DataFurnace software [20]. In-situ real-time RBS was used to investigate diffusion kinetics and stoichiometric evolution, using 2 and 3 MeV H^{++} ions on two selected samples. The samples were sequentially mounted on flat copper surface heating stage with a thermocouple mounted at the back. The thermal annealing was carried out with linear temperature ramping from 160 °C to 600 °C at a rate per minute.

3. Results and discussion

3.1. Microstructural analysis

Fig. 1 shows the surface morphology of the as-deposited samples (a-b) and those of annealed under vacuum (c-d); H/Ar gas mixture and H_2 atmospheres (e-f) and (g-h) respectively. The as-deposited samples, Fig. 1(a) and (b), showed homogeneous smooth surface.

Samples annealed in vacuum (Fig. 1(c–d)) displayed a rough granular surface while those annealed in the presence of H(15%)/Ar(85%) gas mixture (Fig. 1(e–f)) showed a rough surface but with larger coalesced multi-faceted crystals, with thick boundaries as pointed by arrows. The micrographs in Fig. 1(g–h) representing the surface topographic details of samples annealed under pure H_2 gas atmosphere showed, in contrast to samples annealed in the gas mixture, a surface texture similar to the one of as-deposited samples without defined crystals; contrasting to the surface morphology in as-deposited samples however, the surface displays shallow trenches-looking like features that we attribute to the etching effect of hydrogen.

3.2. X-ray diffraction

Fig. 2(a) shows XRD spectra of as-received pure Ti and those of as-deposited multilayer stack on pure Ti substrate as well as of samples on the same substrate annealed in H/Ar gas mixture and in pure H_2 gas. Fig. 2(b) displays analogue spectra in the same sequence where Ti6Al4v alloy replaces Ti.

In both figures, the patterns of both substrates displayed peaks corresponding to the hexagonal α-Ti phase but a new peak corresponding to hexagonal β-Ti phase appeared in the pattern of the Ti alloy substrate. The as-deposited samples on both substrates showed additional diffraction peaks corresponding to Pd. Meanwhile, results from vacuum annealed sample at 550 °C displayed a combination of peaks corresponding to the face-centered cubic (FCC) Pd, hexagonal α-Ti phase and the body-centered cubic (BCC) $PdTi_2$, indicating intermixing of films as a result of thermal annealing.

After annealing at 550 °C in the presence of H(15%)/Ar(85%) gas mixture and pure H_2, XRD spectra of samples on both substrates showed the presence of Ti hydride, the face-centered tetragonal (FCC) TiH_2, in addition to Pd, α- and β-phases observed on the as-deposited samples. Furthermore, the presence of $PdTi_2$ phase in the samples annealed in H (15%)/Ar(85%) gas mixture suggested elemental interfacial diffusion of Pd and Ti. This is in agreement with the work of Topic et al [21] and Fukai [22]. Meanwhile, the absence of this phase in the samples annealed in pure H_2 gas is an indication that there was no intermixing of layers. TiO_2 compound was also observed but only in the samples annealed in H (15%)/Ar (85%) gas mixture atmosphere. However, there was no presence of Pd-hydride; in agreement with the reports of Fujimoto et al. [15] and Adams et al. [23]. Table 2 summarizes the crystallographic information on the phases observed in this XRD investigation.

3.3. Rutherford backscattering spectrometry

The probed depth in this investigation was calculated using SRIM2013 software. For both Ti and Ti6Al4V, the simulation gave a penetration range of ~4.7 μm using 2 MeV He^{++} ions.

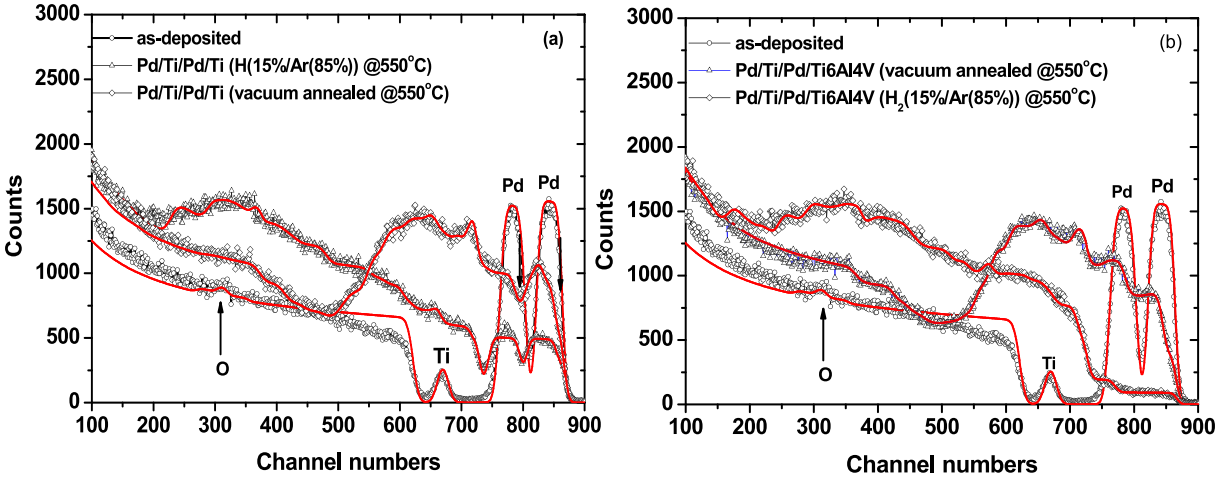

Fig. 3. RBS spectra of the as- deposited compared to those of samples annealed under vacuum, and under H(15%)/Ar(85%) gas mixture on (a) Ti and (b) Ti6Al4V substrates. The simulations are shown in red solid line. (For interpretation of the references to color in this figure legend, the reader is referred to the web version of this article.)

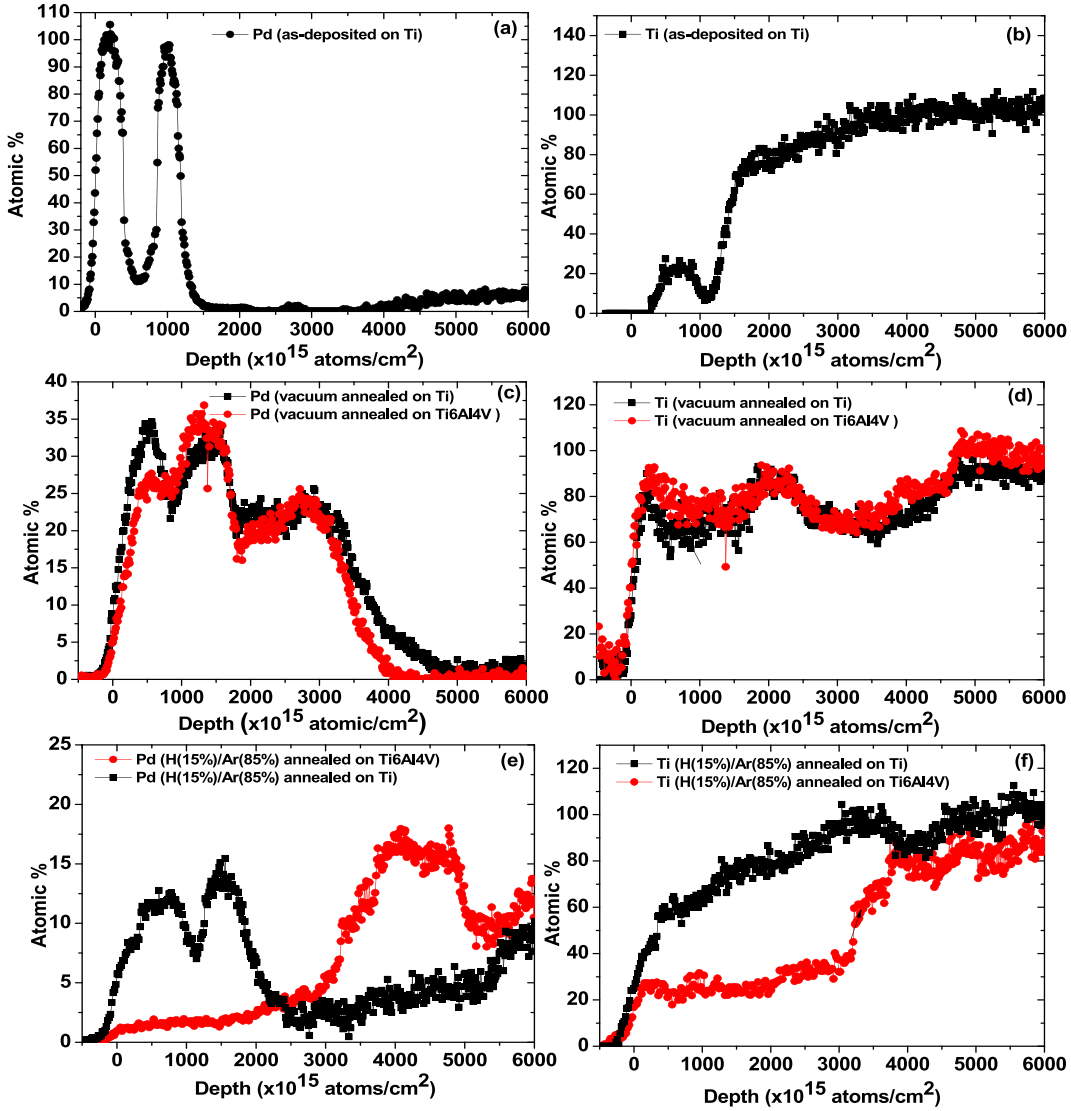

Fig. 4. Depth profiles of Pd (left pane) and Ti (right pane) (a-b) in as deposited samples compared to those in samples annealed (c-d) under vacuum and (e-f) under H_2 (15%)/Ar(85%) gas mixture on Ti and Ti6Al4V substrates.

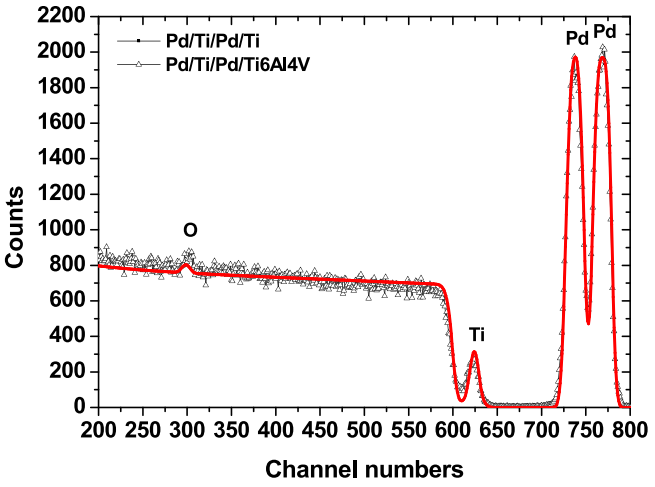

Fig. 5. Experimental and simulated RBS spectra of pure H_2 (100%) annealed samples for one hour.

Fig. 3 shows RBS spectra of samples annealed in vacuum and H (15%)/Ar(85%) gas mixture at 550 °C compared to as-deposited on Ti (Fig. 3(a)) and analogue spectra on the

Ti6Al4V alloy (Fig. 3(b)). As seen on both figures, there was no intermixing of layers in the as-deposited samples. This indicates that there was no spontaneous reaction during deposition.

However, samples, on both Ti and Ti6Al4V, annealed in vacuum displayed intermixing of layers as evidenced by the decrease of Pd counts while counts increased in the rest of the spectra especially in the region between 490 and 750 channels numbers where a visible hump is seen.

Thus the layer intermixing is a result of elemental Pd diffusion. It can also be seen that the drop in Pd counts was sensitive to the substrate; the decrease was pronounced in samples processed on the Ti alloy substrate. Finally we noted the presence of oxygen in the spectra; this is in agreement with XRD results that confirmed the TiO_2 phase.

Fig. 4(a–f) show the depth profiles of Pd and Ti obtained by Data-Furnace software from RBS simulated spectra in Fig. 3(a-b) respectively. Due to similarity of the as-deposited data of samples on both substrates, only one on Ti substrate is presented in Fig. 4(a-b). Irrespective of the substrate, the profiles indicated that Pd atoms diffused inwardly and reacted with Ti; it is enhanced down to a depth of $\sim 2000 \times 10^{15}$ atoms/cm^2 in agreement with XRD analysis where $PdTi_2$ phase was observed. The role of the H(15%)/Ar(85%) gas mixture during annealing can be understood by correlating the SEM micrographs in Fig. 1(e–f) and the Pd diffusion as observed in Fig. 4(c). We noticed a surface roughening with large crystals with clear grain boundaries. This can be explained by the impact of the energetic heated Ar atoms on the surface, which activates the diffusion of Pd atoms onto the Ti layer; the observed grain boundaries may then provide pathways to the diffusing Pd atoms. As the RBS results show a clear depletion of the surface Pd layer, the multi-faceted grains observed in the SEM micrographs are from the Ti rich PdTi mixed layer.

Fig. 5 displays RBS spectra of sample annealed in pure H_2 on Ti substrates (a typical simulated spectrum is also overlaid). Also due to similarity of the data of samples on both substrates, only one spectrum on Ti substrate is presented. A noticeable beneficial effect of annealing in pure H_2 is the preservation of the integrity of the deposited catalyst layers; as a consequence the only new phase formed was TiH_2 as it was observed above by XRD in Fig. 2. Molecular hydrogen is split catalytically by the Pd layer and the formed atomic hydrogen diffuses in the interstitial sites of the sandwiched Ti layer and/or passivates the available Ti bonds; as the Pd layer is preserved in its entirety upon annealing, it appears that the formed TiH_2 phase acts as a diffusion barrier of the catalyst Pd.

Fig. 6 displays in situ real-time RBS spectra showing color coded plots of (a) as-deposited and (b) for the sample annealed in the presence of pure H_2 gas from 160 °C to 600 °C at a rate of 3 °C per minute and the spectra were recorded every 30 s. The plots have been divided into regions for better discussion of the results.

Fig. 6(a) revealed the following:

i. *Region (1):* the reaction and diffusion of atoms of Pd and Ti had not begun; no noticeable change is observed on the spectra of the deposited Pd and Ti layers.
ii. *Region (2):* Pd atoms started to react with Ti but the reaction was very slow as seen by a slight change in the Pd counts. In agreement with the phase diagram of Pd and Ti [24] and the report of Tisone et al [25], the stable $PdTi_2$ and metastable Pd_3Ti phases coexists in the temperature range between 350 °C and 510 °C. According to the same reports the metastable Pd_3Ti phase start to disappear at around 520 °C.
iii. *Region (3):* the two layers are not distinguishable. Our XRD results of samples annealed at 550 °C in Fig. 2 detected the presence of only $PdTi_2$ phase and other related phases. We can conclude that the Pd_3Ti phase is absent above 550 °C.

Fig. 6(b) shows the in-situ real-time RBS plot of the sample annealed under pure H_2. It can be seen that there was no reaction in region 1 up to 400 °C. In region 2, there was a decrease in Pd counts as observed in the buried layer interfacing with the substrate. In region 3, the reaction on the Pd buried layer is seen to accelerate; at the same time the surface Pd layer also dropped in counts but at a lesser extent. We noticed also that the signal in the sandwiched deposited Ti layer is spreading without any noticeable drop in counts. We can summarize and interpret these reactions in region 3 as following:

i. There is a gradual change in color code and spreading of the signal of the Pd buried layer towards the substrate. At the same time, the sub-interface region in the Ti substrate changes in the color code towards lower counts.
ii. The counts in the sandwiched deposited Ti layer are unaffected.

These observations suggest that there is an intermixing between the buried Pd layer and the Ti substrate across the interface. Our XRD results had indicated the formation of TiH_2 phase that acted as a diffusion barrier hindering Pd atoms from the Pd layer on the surface from diffusing inward as reported by Fujimoto et al [15]. The little drop in counts that we observed above 550 °C in the Pd surface layer coupled with a stable counts in the Ti deposited layer suggest that the Ti layer behaved like a permeable membrane to Pd atoms in this temperature range.

3.4. Elastic recoil detection analysis

In this experiment, the penetration range of 3 MeV He^{++} was simulated by SRIM at 75° and was found to be ~1.92 μm. Fig. 7 presents the ERDA spectra of samples annealed under H/Ar gas mixture (Fig. 7(a)) and under pure H_2 (Fig. 7(b)). For the samples annealed under H/Ar gas mixture, ERDA detected a significant surface H component due mainly to hydrocarbon and water vapor, and a low H concentration in the bulk. The H surface component is consistent with our SEM micrographs that showed a rough and grainy surface in these samples. In contrast, for the samples annealed under pure H_2, the H surface component was absent and the H distribution is restricted to the bulk. The absence of H surface component suggests a compact microstructure of the film.

4. Conclusion

Intermixing of the Pd catalyst and the Ti hydrogen absorbing layers has been investigated. For this effect, a Pd/Ti/Pd triple layer stack has

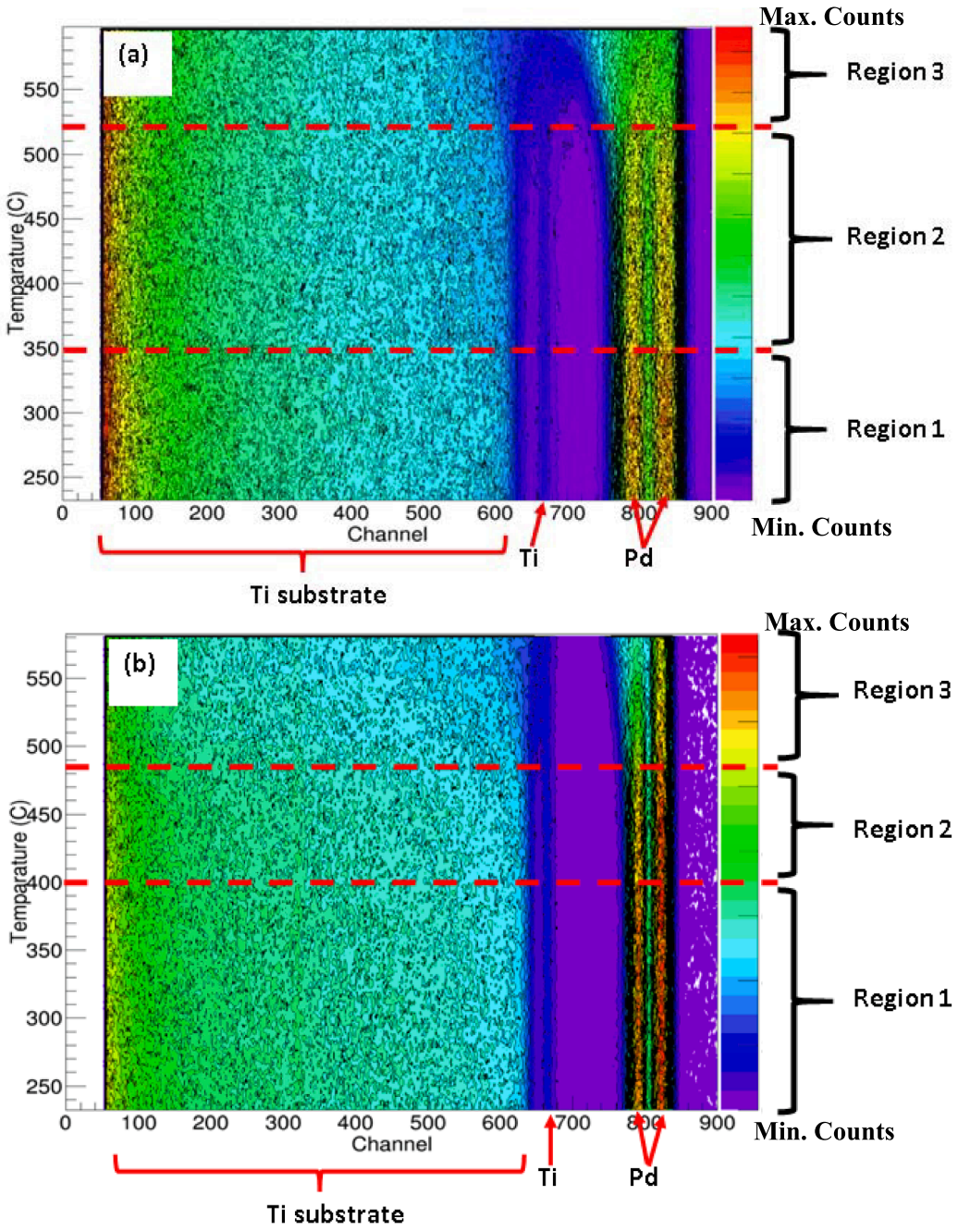

Fig. 6. Color coded in-situ, real-time RBS plot of the total spectra collected from RT to 600 °C. (a) as-deposited sample; (b) pre-annealed sample in the presence of pure hydrogen.

been deposited on Ti and Ti alloy substrates. Both systems were annealed under different atmospheres at the hydrogenation temperature of 550 °C. Under vacuum annealing, XRD has identified the $PdTi_2$ phase formation in the films; RBS confirmed that there was a complete intermixing of the deposited layers. Under H/Ar gas mixture annealing atmosphere in addition to the $PdTi_2$, TiH_2 phase was observed by XRD. RBS study has shown that most of Pd atoms in the two deposited layers diffused inward into the substrate. Under pure H_2 annealing, in comparison to the observations under the H/Ar gas mixture, $PdTi_2$ phase was absent, instead the TiH_2 persist. RBS confirmed indeed that there was no intermixing of the three layers. Based on in-situ real-time RBS finding, we can conclude that the annealing under pure H_2 preserves the integrity of the Pd catalyst

SEM investigation has shown that there was little effect of the substrate on the surface morphology; instead the annealing atmosphere was found to influence it; while the surface of as-deposited samples was found to be smooth, the one of the sample annealed in vacuum was covered by small agglomerate grains. For samples annealed under H/Ar gas mixture, the surface was rough and it showed multi-faceted large crystals with clear grain boundaries. The surface of the annealed samples under pure hydrogen was characterized by a metallic smooth surface similar to that in the as-deposited films; this is consistent to RBS studies that confirmed that the deposited Pd catalyst was not affected upon annealing under pure hydrogen ambient.

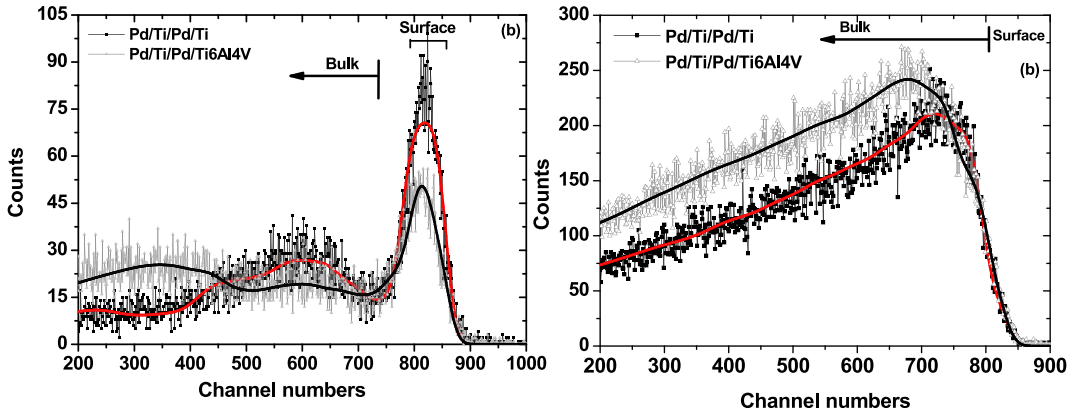

Fig. 7. ERDA spectra of (a) H(15%)/Ar(85%) gas mixture annealed samples, and (b) pure H_2 (100%) annealed samples on Ti and Ti6Al4V alloy respectively; the overlaid solid curves are the simulated spectra.

Declaration of Competing Interest

The authors declare that they have no known competing financial interests or personal relationships that could have appeared to influence the work reported in this paper

Acknowledgements

This work was based on the research supported by the National Research Foundation of South Africa (NRF) via iThemba LABS Materials Research Department (MRD). Authors would like to thank ion beam analysis (IBA) group, software developers, and Tandetron operators for their assistance.

References

[1] N.A.A. Rusman, M. Dahari, A review on the current progress of metal hydrides material for solid-state hydrogen storage applications, Int. J. Hydrogen Energy 41 (28) (2016) 12108–12126.
[2] L.L. Jewell, B.H. Davis, Review of absorption and adsorption in the hydrogen–palladium system, Appl. Catal. A 310 (2006) 1–15.
[3] R.R. Boyer, An overview on the use of titanium in the aerospace industry, Mater. Sci. Eng., A 213 (1996) 103–114.
[4] Z. Tarnawski, N.T.H. Kim-Ngan, Hydrogen storage characteristics of Ti and V based thin film, J. Sci.: Adv. Mater. Devices 1 (2016) 141–146.
[5] E. Tal-Gutelmacher, D. Eliezer, Hydrogen-assisted degradation of titanium based alloys, Mater. Trans. 45 (2004) 1594–1600.
[6] A. López-Suárez, J. Rickards, R. Trejo-Luna, Mechanical and microstructural changes of Ti and Ti–6Al–4V alloy induced by the absorption and desorption of hydrogen, J. Alloy. Compd. 457 (1–2) (2008) 216–220.
[7] Y. Mahajan, S. Nadiv, W.R. Kerr, Studies of hydrogenation in Ti-6Al-4V alloy, Scr. Metall. 13 (8) (1979) 695–699.
[8] I.N. Filimonov, V.V. Yuschenko, A.V. Smirnov, S.N. Nesterenko, I.V. Dobryakova, I.I. Ivanova, E.N. Lubnin, L. Galperin, R.H. Jensen, Deactivation of titanium during temperature-induced hydrogen absorption–desorption cycling: effects of water, oxygen and nitrogen traces, J. Alloy. Compd. 390 (1–2) (2005) 144–154.
[9] S.M. Lee, T.P. Perng, Effect of the second phase on the initiation of hydrogenation of $TiFe_{1-x}M_x$ (M = Cr, Mn) alloys, Int. J. Hydrogen Energy 19 (3) (1994) 259–263.
[10] A. Lopez-Suarez, J. Rickards, R. Trejo-Luna, Analysis of hydrogen absorption by Ti and Ti–6Al–4V using the ERDA technique, Int. J. Hydrogen Energy 28 (10) (2003) 1107–1113.
[11] Y. Baoguo, W. Yujie, Z. Yubin, G. Longqing, Hydrogenation Behaviour of Ti6Al4V alloy rare metal, Mater. Eng. 46 (6) (2017) 1486–1490.
[12] M. Topić, S. Halindintwali, C. Mtshali, S. Nsengiyumva, Z.M. Khumalo, Hydrogen storage in Ti-based metal hydrides investigated by elastic recoil detection analysis (ERDA), Nucl. Inst. Meth. Phys. Res. B 450 (2019) 239–243.
[13] E. Gemelli, N.H.A. Camargo, Oxidation kinetics of commercially pure titanium, Matéria (Rio de Janeiro) 12 (3) (2007) 525–531.
[14] K. Drogowska, S. Flege, C. Schmitt, D. Rogalla, H.W. Becker, N.T. Kim-Ngan, A. Brudnik, Z. Tarnawski, K. Zakrzewska, M. Marszalek, A.G. Balogh, Hydrogen charging effects in Pd/Ti/TiO_2/Ti thin films deposited on Si (111) studied by ion beam analysis methods, Adv. Mater. Sci. Eng. 2011 (2012) 1–8.
[15] Y. Fujimoto, S.M. Tadayyon, O. Yoshinari, K. Tanaka, Effect of hydriding on structural stability of Ni/Ti and Pd/Ti multilayers, Mater. Trans. 38 (9) (1997) 780–786.
[16] Hyo-Ryoung Lim, Nu Si A. Eom, Jeong-Ho Cho, Hong-Baek Cho, Yong-Ho Choa, Hydrogen gettering of titaniumepalladium/ palladium nanocomposite films synthesized by co-sputtering and vacuum-annealing, Int. J. Hydrogen Energy 43 (2018) 19990–19997.
[17] Monika Radlik, Wojciech Juszczyk, Krzysztof Matus, Tomasz Szumełda, Alicja Drelinkiewicz, Zbigniew Karpiński, Generation of palladium silicide in the PdAu-SiO2 nanocomposites during heating in hydrogen, J. Alloy. Compd. 735 (2018) 349–354.
[18] L.C. Feldman, J.W. Mayer, Fundamentals of Surface and Thin Films Analysis, Elsevier Science Publishing Co., Amsterdam, The Netherlands, 1986.
[19] M. Mayer, SIMNRA User's Guide, Garching: Max Planck-Institute fur Plasmaphysik, 2008, 6.0.
[20] N.P. Barradas, C. Jeynes, Nucl. Inst. Meth. Phys. Res. B 266 (2008) 1875.
[21] M. Topic, L. Pichon, S. Nsengiyumva, G. Favaro, M. Dubuisson, S. Halindintwali, S. Mazwi, J. Sibanyoni, C. Mtshali, K. Corin, The effect of surface oxidation on hydrogen absorption in Ti-6Al-4V alloy studied by elastic recoil detection (ERD), X-ray diffraction and nanohardness techniques, J. Alloys Comp. 740 (2018) 879–886.
[22] Y. Fukai, The Metal-Hydrogen System, Basic Bulk Properties, second ed., Springer, 2005.
[23] B.D. Adams, A. Chen, The role of palladium in a hydrogen economy, Mater. Today 14 (6) (2011) 282–289.
[24] H. Okamoto, Pd-Ti (Palladium-Titanium), J. Phase Equilib. Diffusion 34 (2013) 1.
[25] T.C. Tisone, J. Drobek, Diffusion in thin film Ti-Au, Ti-Pd, and Ti-Pt couples, J. Vacuum Sci. Technol. 9 (2014) 1.